*Journal of Applied Electrochemistry* **34**: 1021–1027, 2004.



# Contributions to the ohmic drop in the electrolysis of $ZnCl_2$ in a molten chloride electrolyte

S.C. LANS, A. VAN SANDWIJK and M.A. REUTER*
*Delft University of Technology, Applied Earth Sciences - Resources Engineering, Mijnbouwstraat 120, 2628 RX Delft, The Netherlands*
*(*author for correspondence, fax: +31 15 2782836, e-mail: M.A.Reuter@citg.tudelft.nl)*

Received 18 September 2003; accepted in revised form 15 May 2004

*Key words:* chlorine evolution, electrowinning, image analysis, molten salt, ohmic drop, plume, zinc

**Abstract**

The electrowinning of zinc from zinc chloride with a molten chloride electrolyte was investigated. The electrolysis of zinc chloride shows ohmic limitations. The energy consumption is to a large extent determined by the anodic reaction, the evolution of chlorine. The chlorine gas plume was visualised in a see-through furnace and images were analysed to determine the plume angle. This parameter serves as an input parameter for a model to determine the ohmic contributions of the electrolyte, the plume and a layer of chlorine bubbles sticking to the anode, as well as the plume velocity. The results indicate that the major contribution (~60%) to the ohmic drop is due to a stagnant layer of bubbles growing and sticking to the anode, thereby decreasing the effective anode area by coverage. The plume velocity influences coverage characteristics to some extent, which influences the ohmic drop.

**List of symbols**

| | |
|---|---|
| $A$ | electrode area ($cm^2$) |
| $A:C$ | ratio of anodic to cathodic electrode areas (–) |
| $C_1$ | coverage constant (cm) |
| $C_2$ | constant (–) |
| $d_{gap}$ | inter-electrode distance (cm) |
| $E°$ | standard potential (V) |
| $E_{eq}$ | equilibrium potential (V) |
| $E_{cell}$ | cell potential, difference between anode and cathode potential (V) |
| $\mathscr{F}$ | faradaic constant (96 485 C $mol^{-1}$) |
| $F$ | force (N) |
| $F_B$ | buoyancy force (N) |
| $g$ | gravitational acceleration (cm $s^{-2}$) |
| $H$ | anode height (cm) |
| $h$ | distance from the bottom of the anode (cm) |
| $I$ | current (A) |
| $j$ | current density (A $cm^{-2}$) |
| $L$ | anode width (cm) |
| $M$ | molecular weight (g $mol^{-1}$) |
| $m$ | mass (g) |
| $n$ | number of electrons (–) |
| $p$ | pressure (Pa) |
| $q$ | thickness of covering layer (cm) |
| $R_{gas}$ | gas constant (J $mol^{-1}$ $K^{-1}$) |
| $R$ | resistance (Ω) |
| $T$ | temperature (°C, K) |
| $v$ | plume velocity (cm $s^{-1}$) |
| $V$ | volume ($cm^3$) |
| $W$ | energy consumption (kWh $kg^{-1}$) |

*Greek symbols*

| | |
|---|---|
| $\alpha$ | plume angle (°) |
| $\varepsilon$ | voidage (–) |
| $\phi_m$ | gas production at anode (g $s^{-1}$) |
| $\eta$ | overpotential, $E_{cell} - E_{eq}$(V) |
| $\kappa$ | specific conductivity ($\Omega^{-1}$ $cm^{-1}$) |
| $\kappa_{eff}$ | effective conductivity ($\Omega^{-1}$ $cm^{-1}$) |
| $\rho$ | density (g $cm^{-3}$) |
| $\theta$ | coverage (–) |

## 1. Introduction

An experimental study was carried out on the electrowinning of zinc from a $ZnCl_2$–NaCl–KCl melt. The objective was to investigate the possibility of producing zinc at relatively high current densities and low energy consumption compared to Zn electrolysis from sulphate medium. This paper provides insight of contributions to the ohmic drop, since minimization of the ohmic drop minimizes the energy consumption of the electrowinning process.

Since a patent of 1899 by Swinburne and Ashcroft [1], the electrowinning of zinc from fused zinc chloride media has received attention. The electrowinning reaction is given by:

$$ZnCl_2 \rightarrow Zn(l) + Cl_2(g) \quad (1)$$

The electrowinning according to Reaction 1 has been performed under different conditions, on different scales and with different cell designs [2–14]. It appears that the energy consumption ($W$) lies in the range 1.8–8.8 kWh kg$^{-1}$. The cathodic current density is only limited by the operating temperature and the electrolyte composition, which will solidify locally at the cathode due to depletion of $ZnCl_2$ [15]. Experimental work by Lans et al. [15] has shown that the process is under ohmic control and that the ohmic drop is mainly due to the chlorine evolution at the anode. The data of these experiments have been plotted in Figure 1 with a collection of literature data [5– 7, 10–12, 14]. The reason for the large scatter of literature data can be attributed to the fact that the anode area was never reported correctly. Figure 1 shows that the ratio of anodic to cathodic surface area ($A : C$ ratio) is of great importance.

At relatively small overpotentials, the effective conductivity of the electrolyte is significantly reduced, since the bubbles are non-conductive and reduce the effective electrode area by coverage. A similar effect possibly affects the cell potential in the electrowinning of magnesium from magnesium chloride, since the standard decomposition potential of $MgCl_2$ is 2.51 V at 750 °C, but in practice $E_{cell}$ ranges from 6.0 to 7.5 V at current densities from 0.8 to 1.3 A cm$^{-2}$ [16].

The objective of the present work is to determine the contributions to the ohmic drop by studying the gas plume. Electrochemical methods have been used to characterize the electrowinning.

## 2. Contributions to the cell potential

The cell potential during electrolysis involving gas evolution consists of thermodynamic, kinetic and ohmic contributions. Because the electrolyte consists entirely of chlorides, even at high current densities the concentration of chloride anions at the anode surface will not differ significantly from the bulk concentration. Hence, mass transport will have a negligible effect on the cell potential. Tunold et al. [16] stated that several researchers found no evidence of activation overpotential for the evolution of chlorine in a molten salt, but that the overpotential could be interpreted as an ohmic voltage drop in a surface layer. Furthermore, the bubbles in the bulk electrolyte reduce the effective conductivity of the electrolyte, since the bubbles are non-conductive. The Bruggeman equation (Equation 2) [18] describes the effect of the volume fraction ($\varepsilon$) of non-conducting particles (bubbles) on the effective conductivity, $\kappa_{effective}$, of a mixture non-conducting particles and a conducting solution:

$$\frac{\kappa_{effective}}{\kappa_{electrolyte}} = (1-\varepsilon)^{3/2} \tag{2}$$

As the covered fraction of the electrode surface is electrochemically complete inactive, the true current density, $j_\theta$, is larger than the nominal current density, $I/A_{electrode}$, and will affect the slope of current–potential curves [19]:

$$j_\theta = \frac{I}{A_{electrode}}\left(\frac{1}{1-\theta}\right) \tag{3}$$

The electrolyte between two parallel plate electrodes consists of two sublayers, that is, a layer with bubbles attached to the electrode and a second sublayer with rising bubbles [20]. Janssen [21] concluded that the effective resistance of a solution can be well described by the Bruggeman equation, both for maximum values of $\varepsilon$ in the first bubble layer and in the second bubble layer, respectively. The crowded bubble layer adjacent to the electrode is not removed when solution flow velocities are low [22], meaning that a relatively high ohmic resistance is apparent at low current densities.

On raising the cell voltage to a very high value, a gas film is formed at the anode. This unstable condition and temporary equilibrium is known as the anode effect. Erikson and Tunold [23] investigated the anode effect in chloride melts and found critical current densities in the range of 10–35 A cm$^{-2}$ in multicomponent (Na, K, Ca, Mg chlorides) melts, which are an order of a magnitude higher than the operating current density for electrowinning zinc from zinc chloride (i.e., up to 1.5 A cm$^{-2}$).

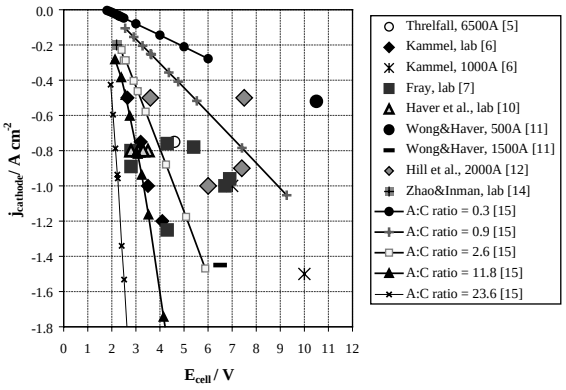


*Fig. 1.* A comparison of the cathodic current density as a function of the cell potential between literature [5–7, 10–12, 14] and own experimental data [15] (different A:C ratio in a $ZnCl_2$–NaCl–KCl electrolyte of 40–30–30 mol % at 450 °C).

## 3. Experimental details

Analytical grade chemicals (stored and handled in a glove box under Ar atmosphere, <1 ppm $O_2$, <1 ppm $H_2O$), were used for the preparation of the solvent. Ternary solvents were used consisting of $ZnCl_2$ with NaCl and KCl, as a 40–30–30 mol% composition, which was determined to be the optimum electrolyte composition with regard to conductivity, surface tension and viscosity [24]. Before the start of an electrometallurgical

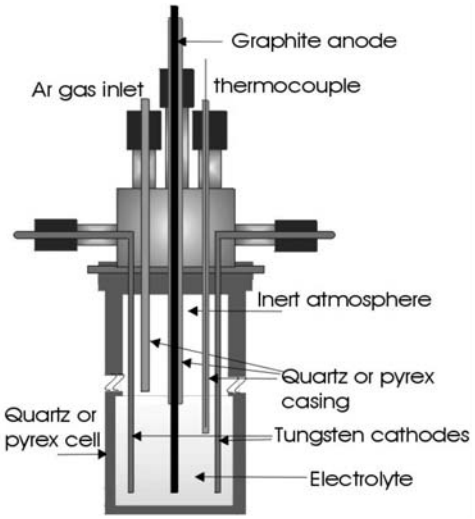


*Fig. 2.* Schematic view of a cross section of the experimental cell.

experiment, the salt mixture was further purified by passing HCl gas (research purity, 99.999%) over the solid and then through the melt, with a flow rate of 40 l $hr^{-1}$ for 3.5 h in total. Subsequently, the gas flow was switched to Ar-gas, which was passed over a $P_2O_5$ filter, before bubbling through the melt.

The electrochemical cell was constructed of quartz and was sealed to control the inner Ar atmosphere. A schematic view of a cross section of the experimental cell is shown in Figure 2. The furnace was heated by a 800 W Kanthal D strip element. The strip of 3 mm width was wound with a 10mm pitch on a quartz tube, which was held in a water-cooled transparent housing, facilitating visual observations. The temperature was controlled (±0.1 °C) by means of a cascade system with K-type thermocouples. The feed forward controller (slave) was of Shinko, type FCR-13A. Temperature control was by means of a Shinko programmable controller (type PC-900).

The electrochemical measurements were carried out with a three-electrode system: an anode with a equidistant cathode at each side (19 mm spacing), facilitating the electrochemical reaction to occur at both sides of the anode. The electrode arrangement of cathode–anode–cathode was used to, as far as possible, ensure current uniformity. The cathodes were constructed out of a tungsten plate of 3.0 cm width, the anode was constructed of a commercial quality of graphite (Carbone Lorriane 4480), also 3.0 cm width and had a thickness of 1.5 mm. The working area of the electrodes was determined by the depth of immersion of the electrodes into the electrolyte and was well controlled at 48 mm. The potential of the tungsten cathodes was measured versus the anode to measure the cell potential using a PGSTAT30 potentiostat, which was used in combination with a BSTR20A current booster (Eco Chemie BV, NL), to enable a high current throughput (20 A). The electrochemical measurement system was fully computer controlled by GPES software.

## 4. Results and discussion

### 4.1. *Current–potential relationships*

Copham and Fray [24] determined that an optimum electrolyte composition for the decomposition of $ZnCl_2$ in a ternary $ZnCl_2$–NaCl–KCl melt is a 40–30–30 mole mixture, the composition used for this work. The cathodic limiting current density was not reached under the conditions of these experiments. Consequently, current–potential relationships for the decomposition of $ZnCl_2$ are linear as shown by Figure 3. The slope is a measure of the conductivity of the electrolyte and the gas voidage. However, the ratio of the effective conductivity ($\kappa_{eff}$) over the theoretical conductivity ($\kappa$, from [24]) decreases for increasing temperature. This is in agreement with the ideal gas law and the Bruggeman equation (Equation 2), that is due to the higher temperature, the gas volume increases, resulting in a lower ratio of $\kappa_{eff}/\kappa$ for a given current density. An increased pressure showed a similar effect on the cell potential and was measured and reported previously by

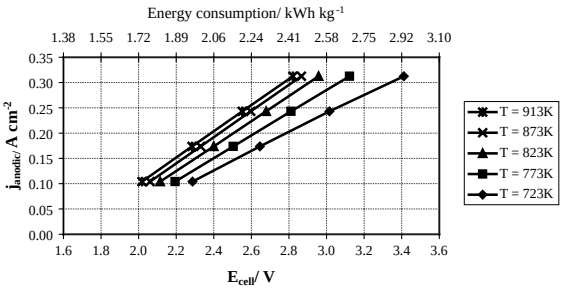


*Fig. 3.* Current density against cell potential for the decomposition of zinc chloride in a $ZnCl_2$–NaCl–KCl melt of 40–30–30 mol % at different temperatures.

*Table 1.* Characteristics for the decomposition of $ZnCl_2$ in a $ZnCl_2$–NaCl–KCl melt of 40–30–30 mol % at different temperatures

| | $T$ = 723 K | $T$ = 773 K | $T$ = 823 K | $T$ = 873 K | $T$ = 913 K |
|---|---|---|---|---|---|
| $E°$/V [25] | 1.61 | 1.57 | 1.54 | 1.50 | 1.48 |
| $E_{eq}$/V | 1.72 | 1.73 | 1.70 | 1.66 | 1.62 |
| $\kappa/\Omega^{-1}$ $cm^{-1}$ [24] | 0.87 | 1.04 | 1.20 | 1.36 | 1.49 |
| $R_{Electrolyte}/\Omega$ | 0.08 | 0.06 | 0.05 | 0.05 | 0.04 |
| $R_{Effective}/\Omega$ | 0.19 | 0.22 | 0.25 | 0.26 | 0.26 |
| $\kappa_{eff}/\kappa$ | 0.41 | 0.28 | 0.22 | 0.19 | 0.17 |

the authors [15]. Table 1 summarises the characteristic values of $\kappa_{eff}/\kappa$ for the experiments at different temperatures. The equilibrium potential ($E_{eq}$) was determined by the cut-off of the linear current–potential relationship of Figure 3, the standard potential of $ZnCl_2$ ($E°$) was determined with HSC thermodynamic software [25].

### 4.2. *Image analysis of the gas plume*

It is postulated that the ohmic drop in the electrolyte with the vertical plate electrodes is dependent on the gas plume. The process was visualized in the see-through furnace, which enabled the measurement of the angle of the gas plume with the anode. A light source was placed behind the see-through furnace. The process was recorded with a Sony DCR-PC100E digital video recorder, resulting in 25 frames per second of 720×576 pixels resolution. The pictures were captured as bitmaps, stored on a personal computer and analysed using graphics software. The mean angle of the plume, $\alpha$, was determined from ten measurements for each stationary situation, of which the highest and lowest measurement were discarded. The standard deviation determined for the eight data points was below 0.5 for all conditions. The results of the measurements are shown by Figure 4. In this experimental set-up, the boundary of the plume seems to be slightly curved, but it was assumed to be valid to approach the representation of the plume by a constant angle $\alpha$, as has been depicted by Figure 5.

## 5. Modelling the plume

To minimize the energy consumption of the electrowinning process, ohmic drop must be minimized. The total cell potential required for electrowinning is simplified to Equation 4, when anodic and cathodic activation and concentration overpotentials are assumed to be negligible, as was argued previously:

$$E_{cell} = |E_{eq}| + |IR| \tag{4}$$

The potential drop term $IR$ represents the energy inefficiencies, due to the resistance, $R$, of the electrolyte between the electrodes, which was derived from the linear $I/E$ relationships. In this case, the volume between the electrodes consists for a significant part of a mixture of electrolyte and gas. The gas hold-up in the electrolyte was characterized by the angle of the plume, $\alpha$. The interelectrode gap can be divided into two parts: that is, with and without gas. In addition, a third part can be assumed, being a stagnant layer of bubbles attached to the anode. A model was developed to discuss how the evolution of chlorine gas affects the ohmic drop, pointing out the problem of a relatively large cell potential, and consequently large energy consumption.

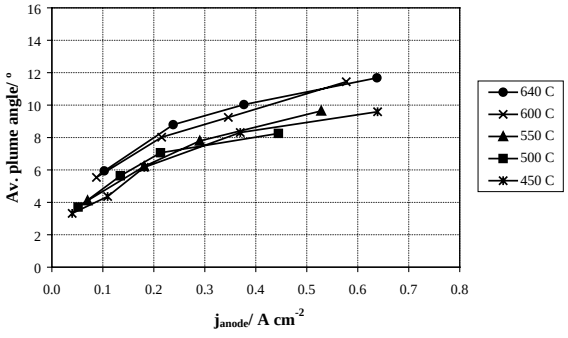


*Fig. 4.* Average angle of plume with anode at different applied cell potentials and temperatures in 40–30–30 mol % $ZnCl_2$–KCl–NaCl electrolyte.

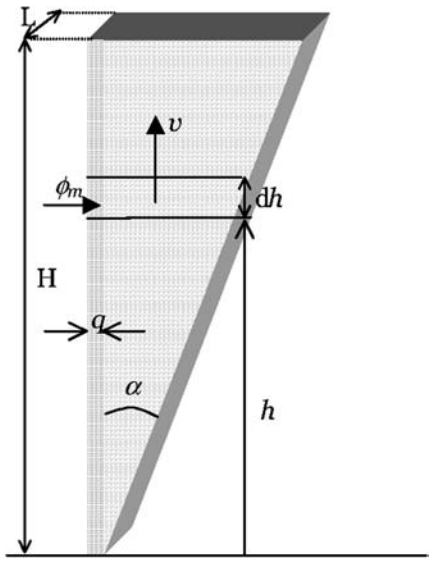


*Fig. 5.* Schematic view of gas plume at the anode.

### 5.1. *Ohmic drop*

The gas plume is assumed to be in a steady state condition. An amount of gas is produced per time unit ($\phi_m$) by a current ($I$), according to the faradaic law. The bubbles that reach the surface of the electrolyte leave the system. A schematic view of the plume with characteristic parameters is shown by Figure 5. Because the experimental set-up was equipped with an anode sided by two cathodes, the depicted view of the plume has a mirrored part as well.

The size of the plume with gas voidage $\varepsilon$ is determined by the following:

(i) the plume height, $H$, equal to the height of the anode
(ii) the plume width, $L$, equal to the width of the anode
(iii) the plume angle, $\alpha$, determined visually as discussed previously
(iv) where $H \tan \alpha$ is smaller than the interelectrode gap.

In addition, a stagnant layer of bubbles at the surface of the anode is assumed, having the following characteristics: a thickness $q$, and the layer covers the anode by a fraction $\theta$.

Subsequently, the overpotential ($\eta$) and resistance ($R$) can be written according to Relation 5. Equations 6 to 8 show that the overpotential between the anode and cathode at an interelectrode distance of $d_{gap}$ is determined by the ohmic drop, which is due to (i) a stagnant layer of bubbles at the anode, of thickness $q (q << d_{gap})$ and covering the anode by a fraction $\theta$ (Equation 6); (ii) the plume, which is a layer of electrolyte, having a conductivity $\kappa$, with voidage $\varepsilon$ (Equation 7); and (iii) the electrolyte without any gas present (Equation 8):

$$\frac{I}{A_{Electrode}} = \frac{E_{cell} - E_{eq}}{R_{Coverage} + R_{Plume} + R_{Electrolyte}} = \frac{\eta}{R_{tot}} \tag{5}$$

$$R_{Coverage} = \frac{q}{\kappa(1-\theta)} \tag{6}$$

$$R_{Plume} = \frac{h \tan \alpha}{\kappa(1-\varepsilon)^{3/2}} \tag{7}$$

$$R_{Electrolyte} = \frac{d_{gap} - h \tan \alpha}{\kappa} \tag{8}$$

The equilibrium potential, $E_{eq}$, has been given by Table 1. Therefore, when Equations 6 to 8 are introduced into Equation 5, the current density at a certain overpotential at a certain height can be defined by Equations 9:

$$\frac{dI}{dh} = \frac{\eta L \kappa C_2}{C_1 C_2 + d_{gap} C_2 + h \tan \alpha - C_2 h \tan \alpha} \tag{9}$$

where:

$$C_1 = \frac{q}{1-\theta} \tag{10}$$

$$C_2 = (1-\varepsilon)^{3/2} \tag{11}$$

The coverage constant, $C_1$, is a measure of the ohmic drop due to bubbles covering the anode, the larger $C_1$, the larger $\theta$ for a certain value of $q$. Solving Equation 9 gives:

$$I = \frac{\eta L \kappa C_2}{(-1 + C_2)\tan \alpha} \ln\left(\frac{C_1 C_2 + C_2 d_{gap}}{C_1 C_2 + C_2 d_{gap} + H \tan \alpha - C_2 H \tan \alpha}\right) \tag{12}$$

The coverage constant $C_1$ can then be determined by solving Equation 12, with a guestimated value of 0.4 for $\varepsilon$. Table 2 gives $C_1$ for an experiment under certain conditions.

The coverage for the projection of a monolayer of bubbles of equal size in a square surface would be $\pi/4$ (or 0.79), therefore, $q$ would be about 6 mm. Although $q$ could not be measured by image analysis, it is not likely that it is this large. A larger value of the coverage $\theta$ is achieved when a bubble distribution exists at the surface of the anode, or that a secondary layer of bubbles is also responsible for shielding the anode. It is reasonable to assume that the moving part of the plume also contri butes to shielding.

*Table 2*. Calculated values of the coverage constant, $C_1$, for different applied cell potentials in a 40–30–30 mol % $ZnCl_2$–KCl–NaCl electrolyte at 550°C

| $E_{cell}$/V | $I/A$ | $\alpha$/° | $C_1$/mm |
|---|---|---|---|
| 2.0 | 2.01 | 4.1 | 29 |
| 2.5 | 5.21 | 6.2 | 30 |
| 3.0 | 8.36 | 7.8 | 31 |
| 4.0 | 15.22 | 9.6 | 28 |

The resistance given by Equations 6 to 8 can be determined separately and it is possible to calculate the contribution of each part to the total ohmic drop. The resulting expressions for the different parts of the ohmic drop are given by Equations 13 to 15.

$$R_{Coverage} = \frac{C_1}{\kappa L H} \tag{13}$$

$$R_{Plume} = \frac{\tan \alpha}{2\kappa C_2 L} \tag{14}$$

$$R_{Electrolyte} = \frac{d_{gap} - H \tan \alpha}{\kappa L H} \tag{15}$$

Modelling the ohmic drop due to gas evolution by this method implies that $R_{tot}$ is constant for each potential or current step, given the linear $I/E$ relationships. $R_{tot}$ and the contributions of $R_{Electrolyte}, R_{Plume}$ and $R_{Coverage}$ are calculated for cell potentials in the range 2–5 V. The coverage constant $C_1$ and $R_{Coverage}$ were used to fit the ohmic $I/E$ relationships and were given a physical meaning, that is a non-moving layer of bubbles.

Figure 6 shows the contributions to the ohmic drop. It shows that the main contribution due to chlorine production is because of chlorine bubbles covering the

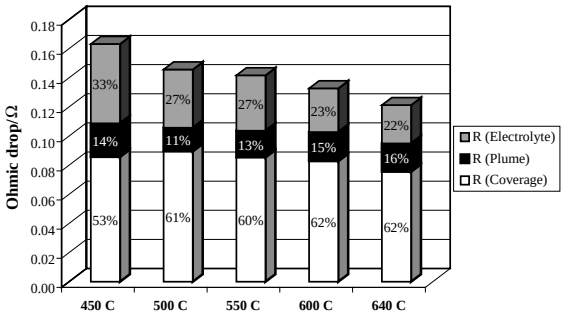


*Fig. 6*. Contributions to the ohmic drop in a 40–30–30 mol % $ZnCl_2$–NaCl–KCl melt at different temperatures.

anode. The contribution of $R_{\text{Electrolyte}}$ can be minimized by decreasing the interelectrode distance. Since the contribution of $R_{\text{Plume}}$ is relatively small, it is postulated that the guestimated value of $\varepsilon$ does not affect the results considerably ($\varepsilon_{\max} = 0.6$, according to ideal sphere packing).

### 5.2. *Plume velocity*

In this Section it is shown by modelling the plume velocity that for increasing current density and increasing plume angle the plume velocity will increase. It can be argued that a higher plume velocity will decrease the contribution of $R_{\text{Coverage}}$, because the action of the plume itself will remove the bubbles at the anode surface.

The plume velocity was modeled by solving the impulse balance in the upward direction, analogously to a model used by Farias and Irons [26] for momentum transfer in an ascending plume. In general, the impulse balance can be defined by

$$\frac{d}{dt}(mv) = \phi_{m,in} v_{in} - \phi_{m,out} v_{out} + \Sigma F = 0 \tag{16}$$

An element of the plume is subject to the following characteristics (Figure 5):

(i) it is a unit electrolyte with voidage $\varepsilon$
(ii) the unit has thickness of $dh$
(iii) it rises with a constant velocity $v$
(iv) the volume of the unit increases, because of the production of gas along the total anode surface, $\phi_m$ ($g\,s^{-1}$). Thus, the surface perpendicular to the flow direction is increasing as a function of height and can be expressed by the plume angle, $\alpha$.
(v) it is assumed that the gas rises with the same velocity as the liquid, the rising velocity being smaller than the terminal velocity, consequently drag forces are not acting and $\Sigma F = F_B$, the buoyancy force.
(vi) the bubble size is assumed to be constant during rise, that means detachment of bubbles from the anode occurs at a certain size and it is assumed that there is no temperature profile and the bubble size is independent of gas pressure, then $v_{in} = v_{out} = v$.

Considering the above, the mass flow in and out of an element of the plume of thickness $dh$ is, respectively, defined by Equations 17 and 18:

$$\phi_{m,in} = (1-\varepsilon)\rho_{liq} L (h \tan\alpha) v \tag{17}$$

$$\phi_{m,out} = (1-\varepsilon)\rho_{liq} L ((h+dh)\tan\alpha) v \tag{18}$$

Thus, the buoyancy force can be derived from the momentum balance for the plume over the total height of the anode ($H$), as shown by Equation 19:

$$F_B = (1-\varepsilon)\rho_{liq} L (H \tan\alpha) v^2 \tag{19}$$

The buoyancy force follows from Archimedes' law and is defined by Equation 20:

$$F_B = \rho g V \quad \text{or} \quad dF_B = (1-\varepsilon)\rho_{liq} g dV \tag{20}$$

The volume of an element of the plume increases with height, because production occurs at the total surface of the anode. The volume of gas is determined by the ideal gas law and increases because of the production term $\phi_m$, at the element of the plume $dh/H$. It is assumed that the gas has the same temperature as the operating temperature. Therefore, the relationship between $dV$ and $dh$ can be given by

$$\frac{dV}{dh} = \frac{h}{v}\frac{\phi_m}{H}\frac{R_{gas} T}{M\, p} \tag{21}$$

Furthermore, the hydrostatic pressure decreases for a rising element of the plume, according to

$$p = p_{atm} + (1-\varepsilon)\rho_{liq} g (H - h) \tag{22}$$

The production term is because of the current and can be expressed by Faraday's law Equation 23:

$$\phi_m = I \frac{M}{n\mathscr{F}} \tag{23}$$

When Equations 21 to 23 are substituted into Equations 20, the buoyancy force can be written as the differential equation:

$$\frac{dF_B}{dh} = (1-\varepsilon)\rho_{liq} g \frac{I}{vH}\frac{R_{gas} T}{n\mathscr{F}}\frac{h}{p_{atm} + (1-\varepsilon)\rho_{liq} g (H-h)} \tag{24}$$

Integration of Equation 24 and equating with Equation 19 gives an expression for the plume velocity, as given by

$$\begin{aligned} v^3 = &-\frac{I}{H^2 L \tan\alpha}\frac{RT}{n\mathscr{F}}\frac{1}{\left((1-\varepsilon)\rho_{liq}\right)^2 g} \\ &- \left((1-\varepsilon)\rho_{liq} g H\right) + p_{atm} \ln\left(\frac{\left(p_{atm} + (1-\varepsilon)\rho_{liq} g H\right)}{p_{atm}}\right) \\ &+ \left((1-\varepsilon)\rho_{liq} g H\right) \ln\left(\frac{p_{atm} + (1-\varepsilon)\rho_{liq} g H}{p_{atm}}\right) \end{aligned} \tag{25}$$

Figure 7 shows a graph of coverage constant ($C_1$) against plume velocity ($v$). The secondary $y$-axis indicates the contribution of the ohmic drop due to coverage to the total ohmic drop. It can be argued that a higher plume velocity results in a decrease in the resistance due

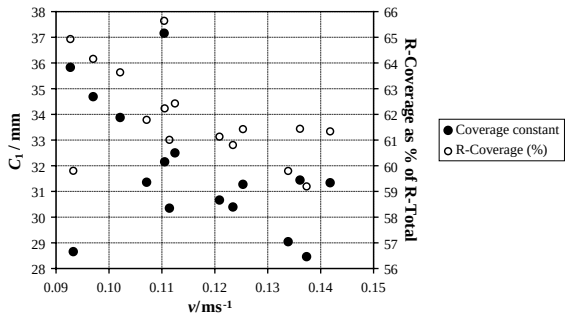


*Fig. 7.* Coverage constant of the anode and contribution of the ohmic drop due to coverage to the total ohmic drop plotted against plume velocity.

to coverage. Apparently, the higher velocity is beneficial for the renewal rate at the surface of the anode. However, unpublished results of this work did not show improved cell performance as a result of mechanical stirring, or gas stirring, probably because convection induced by bubble evolution exceeds the macroconvection of stirring.

## 6. Conclusions

When electrowinning zinc from zinc chloride with a molten salt electrolyte, at relatively small overpotentials the effective conductivity of the electrolyte is significantly reduced. It was found that the formation of chlorine at the anode creates the major part of the ohmic drop, since the bubbles are non-conductive and reduce the effective electrode area by coverage. Electrochemical experiments in a see-through furnace made it possible to depict the chlorine plume at the anode and image analysis proved to be a useful tool to describe the plume. The angle of the plume with the anode was used as an input parameter in a model to determine the coverage of the anode due to chlorine. A very high coverage was determined by the use of the model as well as visual observation through the cell-wall, causing a substantial contribution to the ohmic drop (i.e. about 60%). The resistance due to coverage decreased with increasing plume velocity.

The plume velocity could be determined from the model. The plume velocity is an important process parameter when considering the fluid dynamics in an electrowinning cell. These results may have a significant impact on the design of an industrial electrowinning cell.

## Acknowledgements

The authors would like to acknowledge Umicore and the Institute for the Promotion of Innovation by Science and Technology in Flanders for financial support and discussions.

## References

1. J.W. Swinburne and E.A. Ashcroft, *British Patent 14 278* (1899).
2. E.A. Ashcroft, *US Patent 1 599 269* (1926).
3. E.A. Ashcroft, *British Patent 198 024* (1923).
4. E.A. Ashcroft, *Trans. Inst. Min. Metall.* **43** (1934) 151.
5. R. Threlfall, *J. Soc. Chem. Ind. Trans.* **48** (1929) 210
6. R. Kammel, *Erzmetall* **16** (1963) 113.
7. D.J. Fray, *J. Appl. Electrochem.* **3** (1973) 103.
8. D.E. Shanks, *US Patent 3 962 050* (1976).
9. D.E. Shanks, F.P. Haver, C.H. Elges and M.M. Wong, *Rep. Invest. US Bur. Mines 8343* (1979).
10. F.P. Haver, D.E. Shanks, D.L. Bixby and M.M. Wong, *Rep. Invest. US Bur. Mines 8133* (1976).
11. M.M. Wong and F.P. Haver, 'Fused-salt electrolysis for production of lead and zinc metals', *in* proceedings of int. symp. 'Molten salt electrolysis in metal production', Grenoble, France, 19–21 Sept. (1977) The Instn. Min. Metall., pp. 21–29.
12. S.D. Hill, D.L. Pool and G.A. Smyres, *Rep. Invest. US Bur. Mines 8524* (1981).
13. D. Ferry, Y. Castrillejo and G. Picard, *Electrochim. Acta* **33** (1988) 1661.
14. G. Zhao and D. Inman, *Trans. Nonferrous. Met. Soc. China* **5** (1995) 45.
15. S.C. Lans, A. van Sandwijk, M.A. Reuter, J. Vandenhaute and E.Robert, 'Possibilities of zinc electrowinning from molten chloride salt', *in* Proceedings of 'Chloride Metallurgy 2002' (edited by E. Peek and G. Van Weert). International conference on the 'Practice and Theory of Chloride/metal Interaction', 32nd Annual Hydrometallurgy Meeting, Montreal, Canada, 19–23 Oct. (2002) CIM, pp. 615–628.
16. G.J. Kipouros and D.R. Sadoway, *Adv. Molten Salt Chem.* **6** (1987) 127.
17. R. Tunold, H.M. Bo, K.A. Paulsen and J.O. Yttredal, *Electrochim. Acta* **16** (1971) 2101.
18. D.A.G. Bruggeman, *Ann. Phys.* **24** (1935) 659.
19. J. Eigeldinger and H. Vogt, *Electrochim. Acta* **45** (2000) 4449.
20. C.W.M.P. Sillen, 'The Effect of Gas Bubble Evolution on the Energy Efficiency in Water Electrolysis', Dissertation (Technical University, Eindhoven, The Netherlands, 1983).
21. L.J.J. Janssen, *J. Appl. Electrochem.* **30** (2000) 507.
22. B.E. Bongenaar-Schlenter, L.J.J. Janssen, S.J.D. van Stralen and E. Barendrecht, *J. Appl. Electrochem.* **15** (1985) 537.
23. U. Erikson and R. Tunold, 'On the initiation of anode effect *in* chloride melts', *in* proceedings of international symposium 'Molten Salts' (edited by G. Mamantov, M. Blander, C. Hussey, C. Mamantov, M.L. Saboungi and J. Wilkes), The Electrochemical Society, Vol. 87-7, (1987) pp. 602–612.
24. P.M. Copham and D.J. Fray, *J. Appl. Electrochem.* **21** (1991) 158.
25. A. Roine, 'HSC Chemistry V3.0', Chemical reaction and equilibrium software, Outokumpu Oy, Finland.
26. L.R. Farias and G.A. Irons, *Met. Trans. B.* **17** (1985) 77.